Segmented MEMS Tip-Tilt-Piston Mirrors

Device description, measured characteristics, and application to coherent beam steering

Technology white paper, November 2026

1. Overview

Boston Micromachines Corporation (BMC) manufactures segmented MEMS mirrors developed initially at Boston University (BU) in the laboratory of Thomas Bifano. In these devices, each mirror segment is independently positioned in tip, tilt, and piston using three electrostatic surface-normal actuators, so a surface of N segments presents 3N independent mechanical degrees of freedom.

These surfaces were developed as wavefront correctors for adaptive optics, where the segment array samples and corrects spatial phase error across a pupil. The same three degrees of freedom support a second mode of operation. When tip and tilt are commanded identically across all segments, and piston is set to maintain the correct relative optical phase between them, the array behaves as a single coherent steering mirror rather than as a wavefront corrector. This document describes the hardware and its measured characteristics and treats coherent beam steering as a worked application of it.

Two properties of the actuator determine how the surface is used. The electrostatic actuators are hysteresis-free and highly repeatable, so segment positions can be commanded open loop from a stored calibration rather than held by position feedback. And because the moving element is a single sub-millimeter segment rather than the full aperture, its inertia is low: the steered array exhibits a 27 kHz open-loop −3 dB bandwidth with no resonance peak.

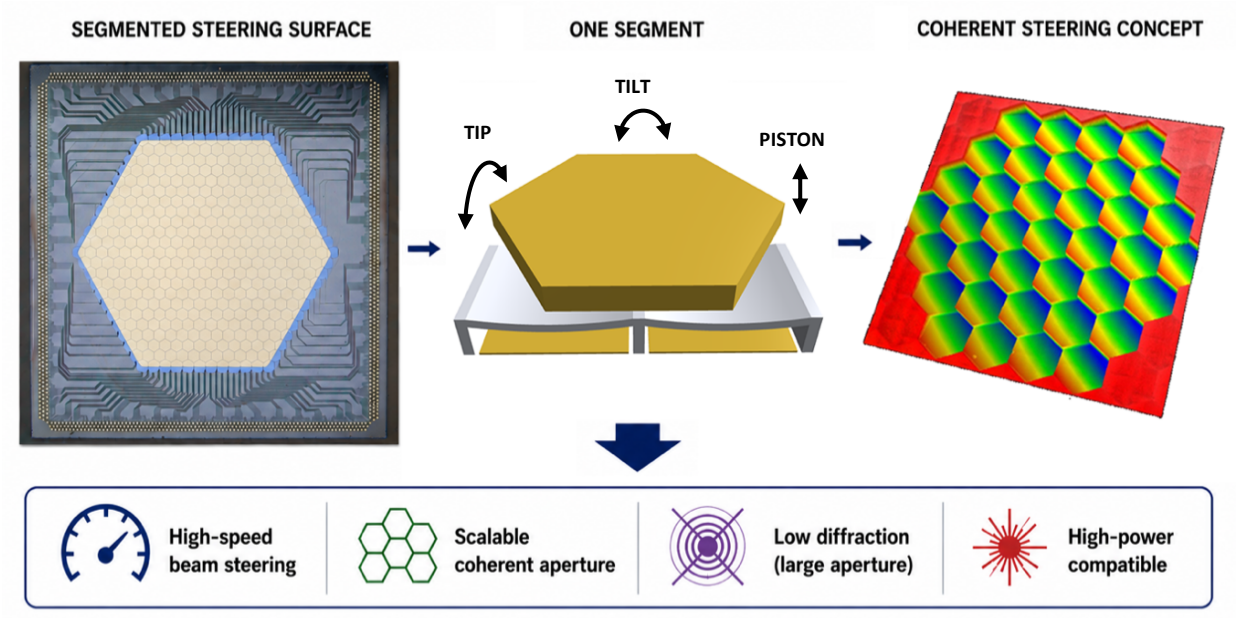


Figure 1 – *Segmented coherent steering surface.* ***Left:*** *Photomicrograph of a gold-coated silicon fabricated segmented steering surface with electrical routing to bond pads at the die perimeter.* ***Center:*** *Each hexagonal segment is supported by three independently actuated electrostatic surface-normal actuators providing calibrated, repeatable tip, tilt, and piston.* ***Right:*** *A single directional command produces coherent open-loop steering of the full array.*

Table 1 summarizes the key measured characteristics, each detailed in the section indicated. Steering and dynamic values were measured on a 37-segment surface at 660 nm at BU; segment figure was measured on a 337-segment surface at BMC.

Table 1 – Summary of segmented steering device characteristics

Parameter	Value	Section
Available formats (segments / actuators)	37 / 111, 337 / 1011, 1022 / 3066	2
Clear aperture	≈ 4.5, 11, 21 mm	2
Fill factor (design)	99.3%	2
Calibrated steering field	±10 mrad optical, 2D	5
Pointing error, open loop, across field	0.71 µrad median (optical)	5
Strehl ratio across field	0.92–0.96 @ 660 nm	5
Residual wavefront error, representative	22 nm RMS	5
Bandwidth, open-loop −3 dB	27 kHz @ 600 µrad tilt amplitude	6
10–90% response / settling to 2%	12 µs / 44 µs	6
Resonance peak	None observed	6
Individual segment figure	8.5 nm RMS surface (17 nm wavefront)	7

2. Device Architecture

These commercially delivered devices are produced by wafer-scale surface micromachining and are available in three standard sizes: **Hex-111** with 37 segments, 111 actuators, 4.5 mm aperture; **Hex-1011** with 337 segments, 1011 actuators, 11 mm aperture; and **Hex-3066** with 1022 segments, 3066 actuators, 21 mm aperture.

The optical surface is a close-packed array of hexagonal mirror segments. Each segment measures approximately 650 µm flat-to-flat and is formed from approximately 15 µm thick epitaxial silicon with a gold reflective coating. Adjacent segments are separated by 2 µm gaps, giving a fill factor of 99.3%.

Each segment is supported by three independently addressed electrostatic surface-normal actuators, each providing approximately 3.5 µm of displacement. The three actuators together define the segment's piston, tip, and tilt: common-mode displacement produces piston, and differential displacement produces angular deflection about two axes. Tilt and piston therefore draw on a shared stroke budget, so the angular range available in each application depends on how much stroke is reserved for phasing.

Actuation is electrostatic and unipolar. An applied voltage displaces the segment toward the substrate, and the segment returns under the restoring force of its own suspension. The mechanism exhibits no hysteresis or creep, and the displacement-voltage relationship is single-valued and repeatable.

Electrical connections are routed from each actuator to bond pads at the die perimeter for attachment to a ceramic package. All three commercial sizes use the same electrostatic actuator architecture and the same wafer-scale fabrication, die-attach, wire-bonding, and packaging processes.

Devices are delivered as a complete unit comprising the packaged mirror, an electronic driver, and a software development kit. The mirror is protected by a window with an antireflective coating.

3. Coherent Beam Steering

Commanding identical tip and tilt across all segments, with piston set to maintain relative optical phase, makes the array behave as a single steering mirror. This is not an array of independently directed beamlets: the segments together form one coherent beam, so all must establish the same outgoing propagation direction while maintaining the phase relationship required for coherent addition. Each segment therefore requires all three degrees of freedom.

The distinction from a conventional fast steering mirror is what moves. An FSM rotates a single mirror spanning the full beam, so its rotational inertia grows as the fourth power of mirror radius and achievable bandwidth falls roughly as the inverse square of beam diameter; compact units in the 10 to 20 mm class typically operate at less than 1 kHz closed loop. In the segmented surface the moving element is one segment, independent of aperture, and it is commanded open loop rather than held by a position servo.

4. Calibration and Control

Measurements of actuators in the device show nearly identical normalized displacement-voltage characteristics. After normalization for stroke, the responses collapse onto a common canonical curve mapping actuator command to displacement. For a 37-segment device with 111 actuators, the variation after normalization was measured to be approximately 2.8 nm RMS. That uniformity, combined with hysteresis-free electrostatic actuation, is what permits the surface to be operated deterministically: a single canonical actuator model, fitted once, predicts the behavior of every actuator on the device to within a few nanometers.

Calibration is a single measurement campaign using an interferometric optical profiler. Each segment is individually driven through the same set of command states while every measurement frame records all segments' tilt and piston, so a segment's own response and any mechanical coupling into its neighbors are measured at the same time. Those data fit one forward model — a canonical actuator curve shared by all 111 actuators, plus per-segment mixing (actuator influences on one another within a segment) and neighbor coupling (segment mechanical coupling through shared actuator anchors) — which is then inverted once, offline, into a lookup table covering the full command range. Operation afterwards is a table lookup, with no iteration and no feedback.

The piston allocation that establishes coherence is wavelength-specific, so the lookup table that is fit from calibration data is tied to a specific design wavelength. Retuning the lookup table to a different wavelength requires only computation using the same measured actuator model, not a new calibration measurement campaign.

5. Measured Steering Performance

Figure 2 shows a representative open-loop steering command executed from the calibrated lookup table and then measured interferometrically. It is one of the 756 states in the field survey described below. Commanded to tilt 8000 µrad optically at an orientation 30° from the x axis, the device produced a pointing error of 0.82 µrad, with 11 nm RMS of residual surface (22 nm wavefront) and a Strehl ratio of 0.945 at 660 nm wavelength. Strehl ratio in this document is computed by diffraction from the measured segmented pupil, not estimated from a Maréchal approximation. The commanded plane is removed by least-squares fit, and the residual is propagated by FFT. The result is referenced to an identically masked unaberrated pupil, so the gap pattern cancels exactly between numerator and denominator. The 99.3% fill factor (f) is then applied separately as f^2, a conservative 1.4% fill penalty. Pointing error is the difference between the commanded and delivered beam direction, where the delivered direction is the least-squares tilt of the measured surface, doubled to give the optical angle. Because the plane is removed before Strehl is computed, pointing and Strehl are independent by construction. All angles in this document are optical, equal to twice the mechanical tilt of the mirror surface.

Figure 3 shows beam quality and pointing error measured on a calibrated 37-segment surface (4.5 mm clear aperture) at 660 nm. The survey covered 756 distinct steering commands distributed across a two-dimensional field of ±10 mrad optical, measured and analyzed as described above. Strehl ratio is between 0.92 and 0.96 across the entire field. The pointing figure is field-wide, not repeatability at a fixed command: commanded open loop to any state within the field, the beam arrives with a median pointing error of 0.71 µrad (optical), with no feedback of any kind.

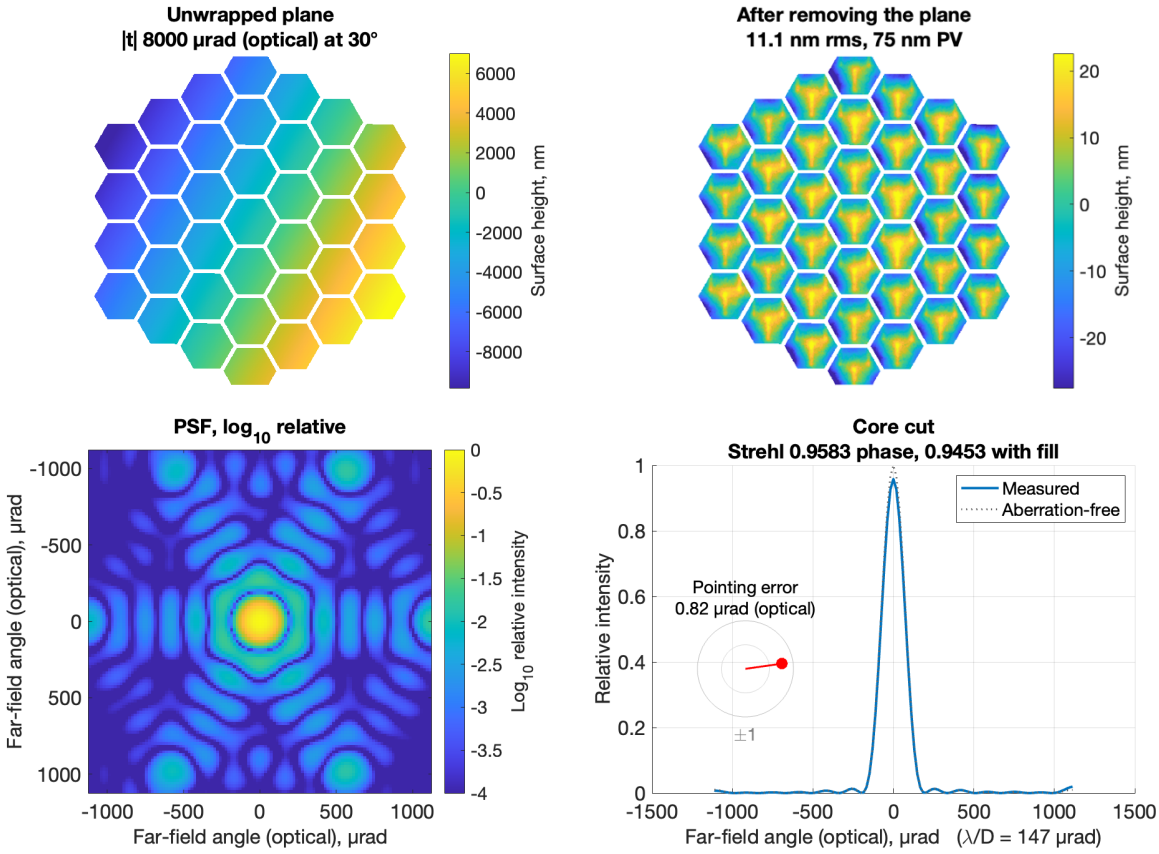


Figure 2 – Representative open-loop steering command from the calibrated lookup table, measured interferometrically: 8000 µrad optical at 30°. Clockwise from top left: unwrapped segment heights; residual topography after removal of the commanded plane (11.1 nm RMS surface, 22.2 nm RMS wavefront); far-field core cut versus the aberration-free case (Strehl 0.945 at 660 nm); far-field pattern on a four-decade log scale. Pointing error is 0.82 µrad against a diffraction width λ/D = 147 µrad.

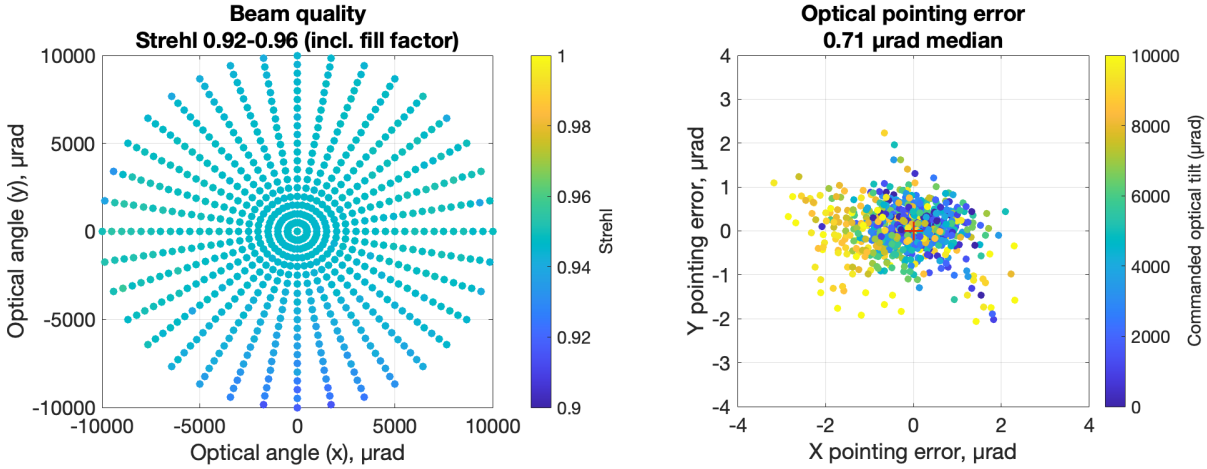


Figure 3 – Measured beam quality and pointing error for 756 commanded steering angles across the ±10 mrad field (37-segment surface, 660 nm). Left: Strehl ratio, computed as described above, between 0.92 and 0.96 across the field. Right: Pointing error, the difference between delivered and commanded optical steering angle, colored by commanded angle magnitude. Median pointing error is 0.71 µrad.

6. Dynamic Response

Temporal response was measured on a 37-segment device with all segments steering coherently. A 660 nm laser reflected from the array was focused onto a quadrant detector, and the steering angle was recorded while the entire array was driven open loop. Figure 4 shows the measured frequency and step responses. The array has a 27 kHz −3 dB bandwidth, a 12 µs 10–90% response time, and 44 µs settling to within 2%, with no observable resonance peak.

This command-following bandwidth is roughly 30× the approximately 900 Hz closed-loop bandwidth of representative commercial piezoelectric fast steering mirrors of similar aperture. It is an open-loop command-following bandwidth, not a demonstrated disturbance-rejection bandwidth.

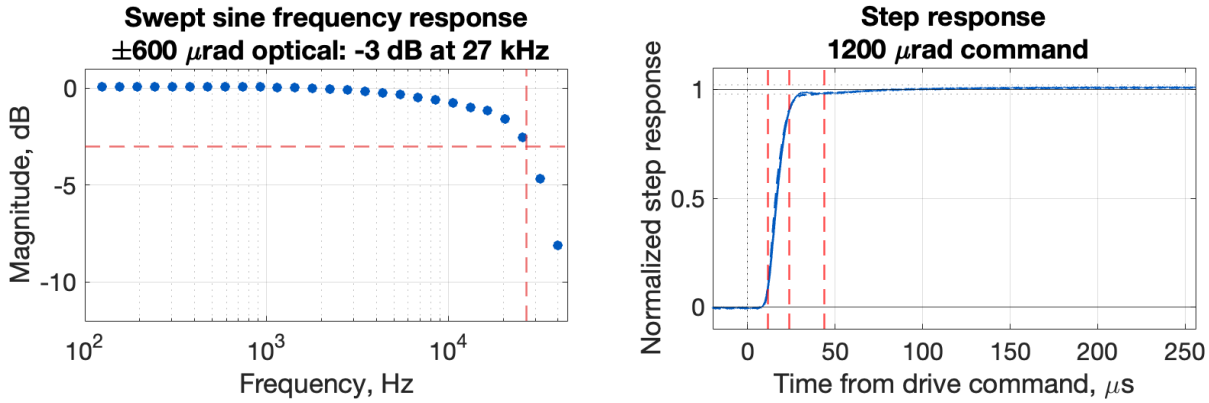


Figure 4 – Measured open loop steering dynamics of a 37-segment mirror with all segments steering coherently. ***Left:*** *Open loop swept sine frequency response, +/-600 µradian optical angle command. Measured -3 dB bandwidth: 27 kHz.* ***Right:*** *Measured response for a 1200 µradian optical angular step. Measured 10–90% response time: 12 µs. Measured settling time within 2%: 44 µs.*

7. Optical Surface Quality

Interferometric characterization of a 337-segment surface separates global wafer-scale figure from local segment-scale error (Figure 5).

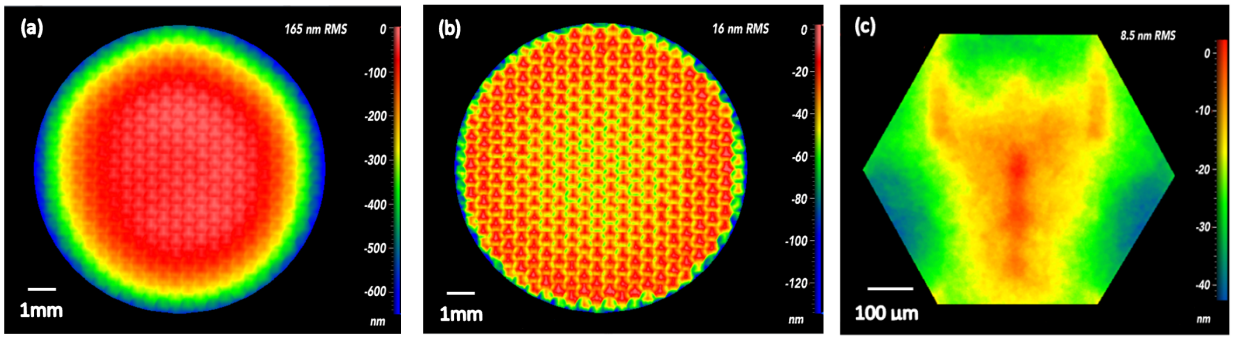


Figure 5 – Static surface characterization of a 337-segment surface. ***(a)****: Measured interferometric surface map of the unpowered device across the active aperture.* ***(b)****: The same map after subtraction of best-fit global curvature and application of a 4 mm period spatial high-pass filter, isolating segment-scale structure.* ***(c)****: Interferometric measurement of an individual mirror segment.*

The dominant contribution to the unpowered figure is low-order global curvature from polishing and residual fabrication stress. Because it is common to the entire aperture and low in spatial frequency, it is readily compensated during alignment or by the optical system, and it is not an intrinsic limitation of the architecture. The residual after its removal demonstrates the wafer-scale coplanarity of the segmented

aperture, and the 8.5 nm RMS figure of an individual segment is well within the requirement for diffraction-limited operation at 660 nm.

8. Optical Power Handling

In a thermal test, the surface of a 37-segment DM was irradiated with a 455 nm LED source, up to a heat load equivalent to 108 W/cm² at 1550 nm (5.5 W/cm² incident at 455 nm, about 3.2 W/cm² absorbed by the gold coating). The mirror performed without problems throughout. At maximum power, the surface reached about 57 °C, up about 32 °C from ambient. Heating scaled roughly linearly with power, and the surface returned to near ambient within a few minutes of shutoff. Strehl ratio was maintained at every heat load, and actuator function and command-versus-position curves showed no measurable change. The 99.3% fill factor leaves approximately 0.7% of incident optical power interacting with the inter-segment gaps, and the disposition of that fraction has not been experimentally quantified. Because the coating incorporates an underlying metallic layer, transmission into the silicon substrate is expected to be insignificant. Quantifying gap-loss thermal effects and scatter is an active characterization objective.

9. Heritage, Production, and Availability

Boston Micromachines Corporation (BMC) was founded in 1999 to commercialize MEMS adaptive-optics technology developed at Boston University and has manufactured electrostatic MEMS deformable mirrors for research, industrial, aerospace, and defense customers for more than 25 years. The company maintains the infrastructure required for production: MEMS design, co-engineered foundry processes, thin-film coating, precision assembly, hermetic packaging, electronic integration, and calibration.

BMC mirrors are deployed in extreme adaptive-optics instruments at Subaru, Gemini, Magellan, and Keck, where they provide diffraction-limited wavefront control under demanding operational conditions. A 1022-segment surface was purchased by the Subaru Telescope for an exoplanet imaging testbed (Figure 6).

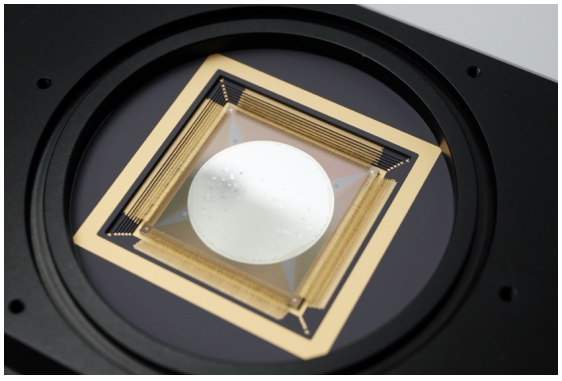


Figure 6 – *Packaged 1022-segment (3066-actuator) segmented surface. The device employs the same electrostatic MEMS actuator technology and fabrication processes as the 37- and 337-segment devices described here.*

The underlying actuator architecture and fabrication process carry substantial environmental heritage. A BMC deformable mirror flew on the MIT DeMi CubeSat, surviving launch, vacuum exposure, and spacecraft thermal cycling before operating successfully on orbit. A BMC subsystem flew on the PICTURE suborbital program, surviving approximately 12 g RMS launch loading and operating above 100 km. JPL total-ionizing-dose testing found no significant degradation in actuation after cobalt-60 exposure to approximately 30,000 Gy. A BMC deformable mirror has been operated at approximately 95 K through five vacuum-thermal cycles with no measurable change from room-temperature performance.

Several of these demonstrations used continuous-facesheet devices rather than the segmented tip-tilt-piston geometry, and none constitutes qualification of an integrated subsystem including drive

electronics. They do establish that the core MEMS technology is compatible with launch, thermal, vacuum, and radiation environments, and that the fabrication process is a production process.